

Counting statistics of ultra-broadband microwave photons

Simon Bolduc Beaudoin, Edouard Pinsolle, and Bertrand Reulet

Département de physique, Institut quantique, Université de Sherbrooke, Sherbrooke, Québec, Canada J1K 2R1

(Dated: August 16, 2024)

We report measurements of counting statistics, average and variance, of microwave photons of ill-defined frequency : bichromatic photons, i.e. photons involving two well separated frequencies, and "white" broadband photons. Our setup allows for the analysis of single photonic modes of arbitrary waveform over the 1-10 GHz frequency range. The photon statistics is obtained by on-the-fly numerical calculation from the sampled time-dependent voltage. Using an ac+dc biased tunnel junction as a source of quantum microwave, we report an ultra-wide squeezing spectrum representing a competitive source for entanglement generation (up to 0.9 billion measured entangled bits per second) easily achievable experimentally. We also report the observation of quantum steering by the tunnel junction, and show how the presence of squeezing of a broadband mode implies the existence of entanglement between two modes it encompasses.

Quantum correlations in the electromagnetic field is a key resource in the development of quantum technologies. Entangled light can substantially improve the signal to noise (SNR) ratio in imaging [1, 2], gravitational wave detection [3] and is currently used to accelerate dark matter research [4].

To achieve high entanglement generation rate in the microwave domain, a great effort has been put into adapting travelling wave parametric amplifiers (TWPA) [5–7] to produce broadband squeezed states. Widening the band over which squeezing occurs increases the number of useful entangled pairs in the signal. Indeed, TWPAs are outperforming Josephson parametric amplifiers (JPAs) by their squeezing bandwidth, from 0.7 GHz[8, 9] to 4 GHz[7], while also promising a large amount of squeezing. While TWPAs are a fascinating and promising technology for the generation of large bandwidth quantum states, they are complex to design and very difficult to fabricate.

Developing broadband sources also requires developing the theoretical and experimental tools to analyse their output field. A usual characterization consists of detecting the quadratures of the field at pairs of frequencies $F - \Delta f$ and $F + \Delta f$ symmetrically situated around F . The central frequency F is related to the frequency f_p of the pump used to generate pairs in the TWPA: $F = f_p/2$ for three wave mixing, $F = f_p$ for four wave mixing. The so-called squeezing spectrum, which measures the amount of squeezing vs. Δf is usually obtained by correlating the quadratures at frequencies $F + \Delta f$ and $F - \Delta f$. Detecting these quadratures requires knowing the phase of the pump, for example to phase-lock a local oscillator used to downconvert the measured signal. But one may want to know whether photon pairs are present in the signal irrespective of any phase reference. This is the case, for example, in experiments utilizing the DC Josephson effect to generate correlations [10–14], or in the more general situation where one does not know the exact conditions generating the signal of interest as for the study of correlations in the cosmic microwave background [15].

In this article we develop another way of analyzing

broadband signals, by measuring the counting statistics of single photonic modes that are not monochromatic but broadband, i.e. with no well-defined frequency. We achieve this goal by numerical treatment of the measured time-dependent voltage, following the theory developed in [16]. We focus on two photonic modes: i) bichromatic photons, i.e. photons of two simultaneous frequencies, and ii) "white" photons, i.e. single modes having a broad frequency content, up to 1 to 10 GHz. Selecting numerically the mode basis is highly flexible and could be particularly useful for coherent wideband emitters such as pulses of sub-cycle duration [17–20]. We chose to work with a normal-metal tunnel junction in the microwave regime (1 to 10 GHz) as a simple wideband emitter to test this method. This device is easy to fabricate, yet provides a quantum radiation with a bandwidth only limited by the RC time of the junction, here > 15 GHz. Indeed, in the presence of a dc+ac bias, such a junction has been predicted to emit broadband squeezed radiation [21], which has been confirmed experimentally on various narrow bands [22, 23]. While using bichromatic modes our technique provides the whole squeezing spectrum of the junction, working with wideband modes allows us to observe squeezing with larger bandwidth and improved signal to noise ratio.

Our experiment also allows also for the measurement of quantum information related correlations for broadband signals: entanglement of formation [24], entanglement generation rate [5, 7] and steering [25, 26]. We indeed observe an entanglement generation rate comparable to TWPAs: the weak amount of squeezing is compensated by the large bandwidth over which photon pairs are generated. We also show that the high frequency part (6-9 GHz) of the spectrum of the radiation of the tunnel junction could steer the low frequency part of it (3-6 GHz).

I. PRINCIPLE OF THE MEASUREMENT

We consider experiments in the microwave domain where a source placed at ultra-low temperature generates an electromagnetic radiation that propagates along

a coaxial cable and is detected by a matched amplifier. In this setup the measured quantity is the time-dependent voltage amplitude of that wave, represented by the operator \hat{v} , superimposed on the noise of the amplification scheme. After further amplification, the signal is digitized at high speed and all the relevant quantities are computed from the digitized signal.

A. First quantization: definition of modes

In order to compute the photon statistics of the signal, one has to define which photons to count. In [16] the chosen basis was that of photons localized in time, at the extreme opposite of the usual first quantization in the frequency domain. In a real experiment, one has to mitigate both approaches by considering wavelets of finite time and frequency spread. We note $\beta(t)$ such wavelets in time domain and $\beta(f)$ in frequency domain; they correspond to the current mode of interest. Since $\beta(t)$ is real, $\beta(-f) = \beta^*(f)$. We start by considering two such wavelets $\beta_{1,2}$ centered around frequencies $f_{1,2}$ that are well separated so that β_1 and β_2 do not overlap. Typically, the width of $\beta_{1,2}(f)$ is $\sim 200\text{MHz}$ whereas $f_2 - f_1$ varies between 1 and 10 GHz. We define the annihilation operators $a_{1,2}$ of photons in the modes $\beta_{1,2}$ by:

$$\hat{a}_{1,2} = \int_0^{+\infty} \beta_{1,2}(f) \hat{a}(f) df \quad , \quad (1)$$

where $\hat{a}(f)$ is the usual annihilation operator for a photon at frequency f . Since the wavelets $\beta_{1,2}(f)$ are narrow in frequency domain, one can simply think of the operators $\hat{a}_{1,2}$ as annihilating photons of frequency $f_{1,2}$ which would correspond to the limit $\beta_{1,2}(f) = \delta(f - f_{1,2})$. The β functions are normalized according to:

$$\int_0^{+\infty} |\beta(f)|^2 df = 1 \quad . \quad (2)$$

since they correspond to single photonic modes (see e.g. [27]). From this we define the annihilation operator for a bichromatic photon,

$$\hat{b} = \frac{\hat{a}_1 + \hat{a}_2}{\sqrt{2}} \quad . \quad (3)$$

This operator annihilates a photon of mode $\beta = (\beta_1 + \beta_2)/\sqrt{2}$. Here the plus sign between the monochromatic annihilation operators $\hat{a}_{1,2}$ is arbitrary. One may consider a minus sign or any complex phase as well (we studied experimentally this for the photon statistics of squeezed radiation, see below). The photon number operator is defined by:

$$\hat{n} = \hat{b}^\dagger \hat{b} = \frac{\hat{n}_1 + \hat{n}_2}{2} + \hat{\Delta} \quad , \quad \text{with } \hat{\Delta} = \frac{\hat{a}_1^\dagger \hat{a}_2 + \hat{a}_2^\dagger \hat{a}_1}{2} \quad . \quad (4)$$

The photocount distribution of bichromatic photons is obtained by calculating the moments of \hat{n} . \hat{n} is distinct

from the total photon number operator $\hat{N} = \hat{a}_1^\dagger \hat{a}_1 + \hat{a}_2^\dagger \hat{a}_2$ (see e.g. Barnett and Radmore [27] chapter 3). The former is a measure of the photon number in a single particular mode of the field as the latter is summed over all modes. Here for example, we can complete the 2-frequency basis by introducing $\hat{c} = (\hat{a}_1 - \hat{a}_2)/\sqrt{2}$ such that $\hat{N} = \hat{b}^\dagger \hat{b} + \hat{c}^\dagger \hat{c}$, $[\hat{b}^\dagger, \hat{b}] = 1$ and $[\hat{b}^\dagger, \hat{c}] = 0$. Since we

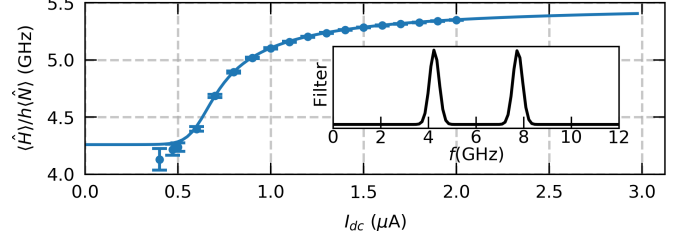


FIG. 1. Total average energy $\langle \hat{H} \rangle$ divided by the total average photon number $\langle \hat{N} \rangle$, in units of frequency in GHz for bichromatic photons (at frequencies $f_1 = 4.25$ GHz and $f_2 = 7.75$ GHz) emitted by the tunnel junction as a function of the dc current bias. Markers are experimental data, solid line theoretical prediction. There is no choice of frequency \bar{f} for which $\langle \hat{H} \rangle = \langle \hat{N} \rangle h \bar{f}$. Data at very low current were omitted since both $\langle \hat{N} \rangle$ and $\langle \hat{H} \rangle$ vanish in this limit. Inset: The numerical filter used for this experiment.

are dealing with broadband signals, the total number of photons \hat{N} and the total energy $\hat{H} = \hbar \omega_1 \hat{n}_1 + \hbar \omega_2 \hat{n}_2$ are not proportional. We illustrate this point experimentally in Fig.1: we measure on one hand the total energy \hat{H} and on another the total photon number \hat{N} of the radiation of a tunnel junction in modes of well separated frequencies $f_1 = 4.25$ GHz and $f_2 = 7.75$ GHz. We plot the "effective frequency" $\langle \hat{H} \rangle / \langle \hat{N} \rangle$ as a function of the current bias in the junction. It is clear that it is not a constant: it varies from ~ 4.2 GHz at low bias to ~ 5.5 GHz at high bias, as a direct result of the radiation being broadband.

B. Quadrature Transform

The link between the measured time-dependent voltage $\hat{v}(t)$ and the photocount statistics is performed by defining the quadrature $\hat{x}(t)$ according to [16] :

$$\hat{x}(t) = \beta \otimes k \otimes \hat{v}(t) \quad , \quad (5)$$

where \otimes is the convolution product and $k(t) = \sqrt{1/(Zh|t|)}$ with Z the impedance of the detector, across which \hat{v} is measured. \hat{x} is the generalization to broadband signals of the usual quadrature of a signal at a given frequency f , i.e. its in-phase component. In frequency space, $\hat{x}(f) = \beta(f)k(f)\hat{v}(f)$ with

$$\hat{v}(f) = -i\sqrt{\frac{Zh f}{2}} \hat{a}(f) e^{-2i\pi f t} + \text{H.c.} \quad . \quad (6)$$

The kernel k is chosen such that $\hat{x}(f) = [\hat{a}(f) + \hat{a}^\dagger(f)]/\sqrt{2}$ and β defines the photonic mode, as discussed above.

More precisely, the kernel $k(t)$ transforms the measured voltage $\hat{v}(t)$ into the quadrature $\hat{x}(t)$ by canceling out the frequency-dependent prefactors which relate \hat{v} to \hat{a} in Eq.(6).

C. Photocount statistics

From the computed time-dependent quadrature, we can deduce the photocount statistics. Herein we focus on the average photon number, $\langle \hat{n} \rangle$, and its variance, $\langle \delta \hat{n}^2 \rangle$, with $\delta \hat{n} = \hat{n} - \langle \hat{n} \rangle$. The procedure is similar to what has been done in [28, 29], although differences arise from the large bandwidth involved here (see appendix B). We find:

$$\begin{aligned} \langle \hat{n} \rangle &= \langle \hat{x}^2 \rangle - \frac{1}{2} \\ \langle \delta \hat{n}^2 \rangle &= \frac{2}{3} \langle \hat{x}^4 \rangle - \langle \hat{x}^2 \rangle^2 - \frac{1}{4}, \end{aligned} \quad (7)$$

where the average over $\hat{x}^2(t)$ and $\hat{x}^4(t)$ is experimentally taken over time. This is a generalization of the theoretical results of [28, 29] for any mode β with certain restrictions concerning non-symmetric (n.s.) terms (i.e. terms that are non-symmetric with respect to conjugation, ex: $\hat{b}^\dagger \hat{b}^3$). These terms are set to be negligible either by construction (choosing $\beta(f)$ such that they are guaranteed to be 0) or by supposing that the light source guarantees $\langle \text{n.s.} \rangle = 0$, which is the case for a tunnel junction.

II. METHODOLOGY

A. Experimental setup

The experimental setup is depicted in Fig. 2. The source of the electromagnetic field is an Al / AlO_x / Al tunnel junction of resistance $R = 52.5 \, \Omega$ fabricated using standard photolithography and e-beam evaporation techniques [30]. It is placed on the cold stage of a dilution refrigerator with a base temperature of 7 mK. The superconductivity in aluminum is suppressed by the stray magnetic field ~ 100 mT of a strong rare earth magnet placed underneath the sample holder. In applications where a magnetic field is undesirable, the superconductivity of the junction could be suppressed e.g. by adding a small amount of magnetic impurities to the aluminum electrodes [31].

The microwave radiation generated by the junction comes out of the high frequency (> 1 GHz) branch of a diplexer pair, then is low-pass filtered (< 11 GHz), goes through a cryogenic 1-12 GHz HEMT (LNF-LNC1-12A) amplifier followed by a room temperature amplifier and is finally digitized using a 10 bit, 32 GSa/sec digitizer with 10 GHz analog bandwidth (Guzik ADP7104), resulting in a 1.25–10.25 GHz total analog bandwidth. The ac excitation reaches the sample through attenuated stainless

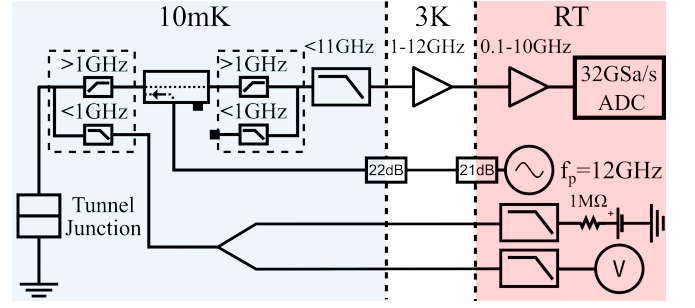


FIG. 2. Experimental setup. On the top is the detection branch, with a bandwidth from 1 to 10 GHz. The middle branch is that of ac bias, with 20 dB of attenuation (43 dB attenuator + 20 dB coupler + 16 dB cables). The lower branch is the dc line, with a current source (a voltage source in series with a $1\text{M}\Omega$ resistor) and a voltmeter to measure the dc voltage across the junction. Both are filtered by a low-pass (6 Hz) filter at room temperature (RT) while thermocoax between RT and the dilution stage strongly attenuate noise above 10MHz. Colors represent the temperature of the various stages: blue is 10 mK, white is 3 K and red is RT.

steel coaxial cables followed by the -20 dB port of a directional coupler. The excitation frequency $f_p = 12$ GHz is above the cutoff of the low-pass filter inserted in the detection line (-17.5 dB insertion loss at 12 GHz), so its weak (-16 dB) reflection on the junction does not affect the measurement by e.g. inducing nonlinearities. The dc ports are low-pass filtered (< 6 Hz) at room temperature before reaching the sample through Thermocoax cables (< 1 MHz) all the way between room temperature and the 7 mK stage.

a. Achieving very low temperature without circulators. Special care was crucial to reach an extremely low electron temperature $T_e < 20$ mK. A first diplexer in front of the amplifier removes the low frequency noise (0-1 GHz) generated by the amplifier. A second diplexer connected to the sample plays the role of a bias tee without adding noise. Caution has been taken to avoid ground loops, in particular those involving the cryogenic amplifier's power supply and the communication channels (USB, etc.).

b. Calibration The power gain and electronic temperature, T_e , are continuously measured and fitted from the full spectrum of current auto-correlations, as in [5, 23, 30, 32]. The only critical calibration parameter needed to recover photon statistics is the gain (between the sample and the A/D converter) as it is used in the kernel for numerical deconvolutions (see Eq.(8) and appendix C). The tunnel junction's electronic temperature and resistance and the loss on the ac port at 12 GHz are only necessary to be able to compare our measurements to the expected emission of the tunnel junction. The average T_e is ~ 17 mK (see Appendix E), with minor fluctuations (~ 0.7 mK) between experiments and the junction resistance was measured to be $52.5 \, \Omega$. Fluctuations in the noise temperature of the amplification chain

are canceled out by alternating experimental conditions with references ($I_{dc} = 0, I_{ac} = 0$). Finally, the attenuation along the ac port at 12 GHz (~ -79 dB) is estimated by fitting the photo-excited auto-correlation, [32].

c. Nonlinearities. The statistics of the voltage fluctuations generated by the sample are separated from that coming from the measurement setup by exploiting the linearity of cumulants for statistically independent variables, $\langle\langle (X + Y)^k \rangle\rangle = \langle\langle X^k \rangle\rangle + \langle\langle Y^k \rangle\rangle$ [28, 29, 32, 33]. This holds true only if the amplification chain is linear enough, as nonlinearities introduce artificial correlations between the noise of the sample and that of its detection. This effect worsens the higher the statistics and it is much preferable to minimize nonlinearities before acquisition than to rely on error-prone post-processing corrections. In our experiment, the main source of non-linearity was traced down to the A/D converter of the digitizer (see Appendix D) and was mitigated by reducing by 6dB the gain in the digitizer itself, i.e. we reduce the width of voltage distribution seen by the digitizer by half, essentially using 9 of the 10 available bits. This sacrifice in dynamic range for linearity effectively resolved all nonlinearity-related issues in measurements, rendering further corrections unnecessary for the presented data.

B. Numerical methods

The 32 GSa/sec voltage samples are numerically converted to photon quadrature using a homemade C++ implementation of the overlap-add method using FFTW for high performance hardware specific FFTs and parallelisation on a 36 cores (Dual Xeon E5-2697v4) server (see github.com/SimonBolducBeaudoin/Time_quadratures). Results shown herein require long averaging (for example, Fig. 4 took ~ 2 weeks of continuous averaging) This is because i) the sample noise represents only between 0.25 and 5% of the total noise of the system, depending on the bias, and ii) we are interested in statistics up to the 4th order cumulant, C_4 . Maximizing throughput helps both for faster experimental iterations and easier compensation for fluctuations in the setup properties (noise temperature fluctuation of the cryogenic amplifier, electrical noise from the power lines, etc.). The numerical convolutions with kernels of 257 points (number of time bins in $k \otimes \beta(t)$) runs at about 2.0 GSa/sec (1 sample is 10 bit) and a typical experimental loop (setting parameters, acquisition, transfer, numerical treatment) runs at an effective sample rate of 1.5 GSa/sec.

The digitized signal is deconvolved to remove the effect of the transfer function from the sample to the digitizer,

$$x(t) = \underbrace{k \otimes \beta \otimes |g|^{-1}}_{\text{numerical}} \otimes \underbrace{g \otimes [v_s(t) + v_A(t)]}_{\text{physical}} \quad , \quad (8)$$

where k identifies the kernels transforming $\hat{v} \rightarrow \hat{x}$, g is the voltage gain between the sample and the digitizer,

v_s is the sample's voltage and v_A is the voltage fluctuation added by the detection. No phase information is contained in our measurement of the power gain, hence we only deconvolve for the modulus of the transfer function, $|g(f)|$. This is enough as long as we consider only even order cumulants that only involve modulus squared of the voltage fluctuations, see below. A numerical kernel $k \otimes \beta \otimes |g|^{-1}$ is constructed for each mode during calibration and is reused during the experiment for each experimental condition. It is noteworthy that since $k \sim 1/\sqrt{|t|}$ contains poles both at $k(t=0)$ and $k(f=0)$ it needs to be regularized, see appendix A. As pointed out in [16], k is not causal: $x(t)$ depends of future times. This is the price to pay to extract photon statistics from traces of the time-dependent voltage.

III. RESULTS

A. Bichromatic thermal radiation

We first test our experiment by measuring the photocount statistics of thermal radiation in a bichromatic single photonic mode, at 4GHz and 8GHz. The radiation comes from the current noise of the tunnel junction when dc biased. While the tunnel junction's noise is not Gaussian, cumulants of order 3 and above are very small so the radiation generated by the junction is almost identical to the thermal one. Changing the dc bias on the junction increases the average photon number, like increasing the temperature does, but the link between the variance and average photon numbers remains the same: $\langle \delta \hat{n}^2 \rangle = \langle \hat{n} \rangle (\langle \hat{n} \rangle + 1)$. This is true provided the statistics is performed on a single mode, irrespective of this mode being narrow-band or not. In Fig. 3 we show the measurements of $\langle \hat{n} \rangle$ (in inset) and $\langle \delta \hat{n}^2 \rangle$ as a function of the dc bias current in the junction for the monochromatic modes \hat{a}_1 at frequency $f_1 = 4$ GHz (red markers), \hat{a}_2 at $f_2 = 8$ GHz (blue) as well as for the bichromatic mode $\hat{b} = (\hat{a}_1 + \hat{a}_2)/\sqrt{2}$ that encompasses both frequencies (cyan). The average photon number in the mode β emitted by the junction is given by [34]:

$$\langle \hat{n} \rangle = 2 \int_0^{+\infty} |\beta(f)|^2 \left(\frac{S_2(f)}{R\hbar f} - \frac{1}{2} \right) df \quad , \quad (9)$$

with $S_2(f)$ the current noise spectral density of the junction at frequency f . The factor two in front of the integral is inserted since $S_2(f)$ is usually defined for positive and negative frequencies. Solid lines for \hat{n}_1 and \hat{n}_2 in the inset of Fig.3 correspond to this formula. The average number of bichromatic photons is obviously given by $\langle \hat{n} \rangle = (\langle \hat{n}_1 \rangle + \langle \hat{n}_2 \rangle)/2$ (cyan solid line). Solid lines in Fig. 3 correspond to $\langle \hat{n} \rangle (\langle \hat{n} \rangle + 1)$. They closely follow our experimental data even in the bichromatic case, indicating that we are correctly counting bichromatic photons.

Let us now consider the operator $\hat{N}/2 = (\hat{n}_1 + \hat{n}_2)/2$, the mean of photon number in modes 1 and 2. Its aver-

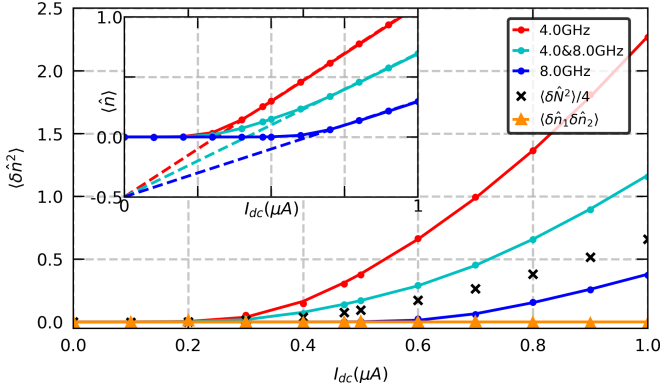


FIG. 3. Variance of the photon number vs. dc current in the junction. Red (resp. blue) ‘.’ markers correspond to monochrome modes at frequency $f_1 = 4$ GHz (resp. $f_2 = 8$ GHz); cyan ‘.’ markers correspond to the bichromatic mode at 4&8 GHz. black ‘x’ markers correspond to $\langle \delta \hat{N}^2 \rangle / 4$ with \hat{N} the total number of photons at frequencies f_1 and f_2 ; orange ‘△’ markers correspond to the correlation $\langle \delta \hat{n}_1 \delta \hat{n}_2 \rangle$. Solid lines are theoretical predictions: $\langle \hat{n} \rangle (\langle \hat{n} \rangle + 1)$. Inset: average photon number vs. dc current in the junction. By extrapolating the linear shot noise regime to the origin (dashed lines) we get the value in photons for vacuum fluctuations ($1/2$ photon for any mode), $\hat{n} + 1/2 = \hat{x}^2 + \hat{p}^2$.

age value is the same as that of the single mode photon number \hat{n} . Its variance is given by:

$$\frac{1}{4} \langle \delta \hat{N}^2 \rangle = \frac{1}{4} (\langle \delta \hat{n}_1^2 \rangle + \langle \delta \hat{n}_2^2 \rangle) + \frac{1}{2} \langle \delta \hat{n}_1 \delta \hat{n}_2 \rangle. \quad (10)$$

The last term, $\langle \delta \hat{n}_1 \delta \hat{n}_2 \rangle$, corresponds to correlations between photons emitted at different frequencies. There are no such correlations in thermal light, as confirmed experimentally, see the orange ‘△’ markers in Fig.3. Then Eq.(10) reduces to the fact that if two random variables are uncorrelated, their variances add. The measurement of $\langle \delta \hat{N}^2 \rangle / 4$ is plotted as black ‘x’ markers in Fig. 3: it clearly differs from $\langle \delta \hat{n}^2 \rangle$ and does not obey the photon statistics of thermal light. The difference between the two comes from the operator $\hat{\Delta}$ introduced in Eq.(4). $\hat{\Delta}(t)$ oscillates at frequency $f_2 - f_1$ and is zero in average. Thus it does not contribute to the average photon number. However $\langle \hat{\Delta}^2 \rangle \neq 0$ contributes to $\langle \delta \hat{n} \rangle^2$ to make it obey the statistics of thermal light. This term reflects the fact that electromagnetic field adds, $\hat{b} \propto \hat{a}_1 + \hat{a}_2$, not the photon numbers, $\hat{n} \neq \hat{n}_1 + \hat{n}_2$.

B. Bichromatic single mode squeezed radiation

In the presence of an ac excitation, the tunnel junction emits a two-mode squeezed radiation by noise modulation [21, 22]. We consider the case where a dc voltage $V_{dc} = hf_p/(2e)$ is superimposed on a sine wave at frequency $f_p = 12$ GHz. In these conditions the junc-

tion emits pairs of photons at frequencies f_1 and f_2 such that $f_1 + f_2 = f_p$ (three wave mixing) where f_1 and f_2 can take any value between 0 and f_p [23]. Hereunder we consider the counting statistics of photons in the bichromatic mode b , as above. If the junction emitted pure squeezed vacuum, one would have the photocount variance given by $\langle \delta \hat{n}^2 \rangle = 2 \langle \hat{n} \rangle (\langle \hat{n} \rangle + 1)$, i.e. the double of that of thermal light[27]. The junction however does not emit only pairs of photons since $\langle \hat{n}_1 \rangle \neq \langle \hat{n}_2 \rangle$. The photocount variance has been measured in the limit $f_1 \simeq f_2$ where the two sidebands were not resolved, i.e. in the limit of single-mode squeezing[29]. Here we extend these results to well separated frequencies $f_1 = 4$ GHz and $f_2 = 8$ GHz. We characterize $\langle \delta \hat{n}^2 \rangle$ by defining the Fano factor $\mathcal{F} = \langle \delta \hat{n}^2 \rangle / \langle \hat{n} \rangle$. For thermal radiation, $\mathcal{F} = \langle \hat{n} \rangle + 1$. We show in Fig. 4 Fano factors vs. $\langle \hat{n} \rangle$

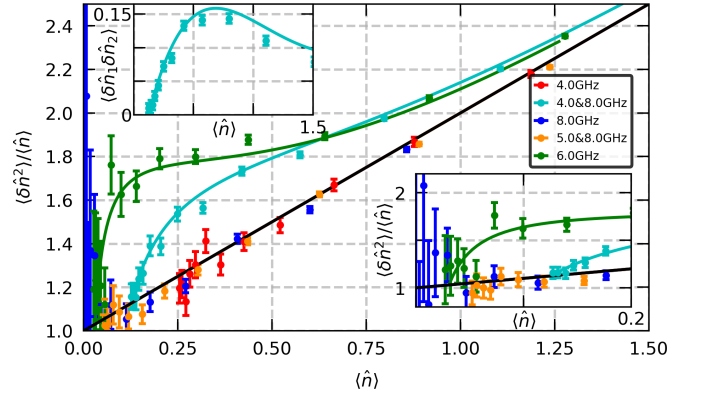


FIG. 4. Fano factor as a function of the average photon number for different photonic modes. Markers are experimental data, solid lines theoretical predictions. Thermal state (black solid line) i.e. $\mathcal{F} = (\langle \hat{n} \rangle + 1)$. Theory for monochromatic modes at 4 GHz (red), 8 GHz (blue) as well as for the 5&8 GHz mode (orange) correspond to thermal light. The average photon number is varied by varying the amplitude of the ac drive at frequency $f_p = 12$ GHz with a constant dc bias $V_{dc} = hf_p/(2e)$. Upper left inset: Correlation between photon numbers at 4 and 8 GHz vs. average bichromatic photon number. Lower right inset: A close-up view of the leftmost part of the graph.

for various amplitudes of the ac drive and various detection modes. If one detects only one frequency, such as 4 GHz (red) or 8 GHz (blue) which do not contain pairs of photons, one obtains thermal statistics (black), as well known for two-mode squeezed light[27]. A bichromatic mode made of two frequencies that do not add up to 12GHz, such as 5 GHz and 8 GHz follow the same statistics (orange). The result for a monochromatic detection at 6 GHz (green) shows a clear deviation from $\langle \hat{n} \rangle + 1$. It corresponds to the result reported in [29] with a lower electronic temperature. The cyan markers correspond to the case $f_1 = 4$ GHz, $f_2 = 8$ GHz: this bichromatic mode indeed bares the signature of the correlations existing between the electromagnetic fields at frequencies f_1 and f_2 , characteristic of two-mode squeezed radiation. Theoret-

ical expectation for squeezed condition, 6 GHz (green) and 4&8 GHz (cyan), are computed from the variance and fourth cumulant of current fluctuations as described in [23, 34].

The photocount variance can be rewritten as:

$$\langle \delta \hat{n}^2 \rangle = \langle \hat{n} \rangle (\langle \hat{n} \rangle + 1) + \langle \delta \hat{n}_1 \delta \hat{n}_2 \rangle. \quad (11)$$

As clear from this expression, the deviation from the statistics of thermal light uniquely comes from correlations between photons at frequencies f_1 and f_2 . In the case of pure squeezed vacuum, only pairs are emitted so $\langle \hat{n} \rangle = \langle \hat{n}_1 \rangle = \langle \hat{n}_2 \rangle$ and $\langle \delta \hat{n}_1 \delta \hat{n}_2 \rangle = \langle \delta \hat{n}_1^2 \rangle$, i.e. the Fano factor is doubled as compared to thermal light. In our experiment the junction emits pairs of photons [35], see the inset of Fig. 4, but not only.

The two measurements discussed until now were meant to demonstrate the ability of our experiment to measure the photocount statistics of broadband signals, in particular bichromatic ones with far apart frequencies. In the following we will apply it to explore some of the potential it offers to analyze more generally broadband radiation.

C. Squeezing spectrum

Analyzing two-mode squeezed radiation at far apart frequencies may be performed by detecting the variance of two quadratures (in-phase and out-of-phase) at each frequencies f_1 and f_2 , i.e. $\hat{X}_{1,2}$ and $\hat{P}_{1,2}$, which are combined into $\hat{X} = (\hat{X}_1 + \hat{X}_2)/\sqrt{2}$ and $\hat{P} = (\hat{P}_1 + \hat{P}_2)/\sqrt{2}$. Correlations between quadratures at different frequencies, for example $\langle \hat{X}_1 \hat{X}_2 \rangle$ lead to the joint quadrature \hat{X} having a variance below that of vacuum, i.e. $\langle \hat{X}^2 \rangle < 1/2$. This procedure usually requires having phase coherence between the detection at f_1 and f_2 as well as the excitation at f_p that leads to the generation of squeezed vacuum by the sample, whatever it is [36]. In contrast, our technique does not require such stringent experimental constraints and is extremely frequency agile in the sense that analyzing another pair of frequencies only requires changing a single line of code. In fact, all the frequencies can be analyzed in parallel with a single acquisition. Our method however provides photocount statistics, not the variance of the quadratures. Below we show how these can be deduced from our measurements, which allows us to measure the squeezing spectrum of a broadband radiation [37, 38].

The quadratures at single frequencies f_1, f_2 correspond to the operators $\hat{X}_{1,2} = (\hat{a}_{1,2} + \hat{a}_{1,2}^\dagger)/\sqrt{2}$ and $\hat{P}_{1,2} = -i(\hat{a}_{1,2} - \hat{a}_{1,2}^\dagger)/\sqrt{2}$. Considering again the bichromatic mode $\hat{b} = (\hat{a}_1 + \hat{a}_2)/\sqrt{2}$, the joint quadratures \hat{X} and \hat{P} can be expressed as a function of \hat{b} and \hat{b}^\dagger as : $\hat{X} = (\hat{X}_1 + \hat{X}_2)/\sqrt{2} = (\hat{b} + \hat{b}^\dagger)/\sqrt{2}$ and $\hat{P} = (\hat{P}_1 + \hat{P}_2)/\sqrt{2} = -i(\hat{b} - \hat{b}^\dagger)/\sqrt{2}$. This simply means that the two-mode squeezed state involving the modes \hat{a}_1 and \hat{a}_2 is in fact a single-mode squeezed state in terms of \hat{b} .

We now show how to deduce the variance of the two quadratures knowing the photon statistics for a mode \hat{b} of any frequency content, not only bichromatic. Introducing the usual operator $\hat{m} = (\hat{b}^2 + \hat{b}^{\dagger 2})/2$, one has[38]:

$$\hat{n} = \frac{1}{2}(\hat{X}^2 + \hat{P}^2 - 1) \quad (12)$$

$$\hat{m} = \frac{1}{2}(\hat{X}^2 - \hat{P}^2). \quad (13)$$

\hat{m} being sensitive to a global phase in \hat{b} , we choose it so $\langle \hat{b}^2 \rangle$ is real and positive, i.e. so $\langle \hat{m} \rangle = \langle \hat{b}^2 \rangle$. Supposing that \hat{b} is Gaussian and applying Wick's theorem to calculate $\langle (\hat{b}^\dagger \hat{b})^2 \rangle$, we find:

$$\langle \delta \hat{n}^2 \rangle = \langle \hat{n} \rangle (\langle \hat{n} \rangle + 1) + \langle \hat{m} \rangle^2 \quad (14)$$

which allows us to deduce $\langle \hat{m} \rangle$ from the photon statistics. $\langle \hat{m} \rangle$ measures the difference between the variance of \hat{n} and its value for thermal radiation. In the case of the bichromatic mode, and using Eq.(11), one has: $\langle \hat{m} \rangle^2 = \langle \delta \hat{n}_1 \delta \hat{n}_2 \rangle$, i.e. $\langle \hat{m} \rangle$ is also a measurement of the correlations between photons at frequencies f_1 and f_2 .

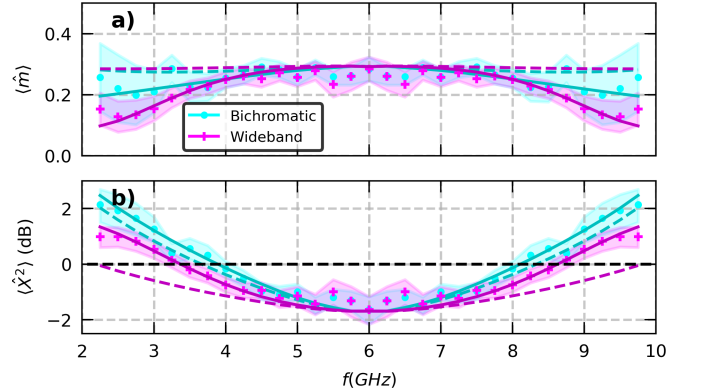


FIG. 5. $\langle \hat{m} \rangle$ in linear scale (a) and variance of the quadrature X in dB referred to vacuum (b) as a function of frequency f for a tunnel junction excited at frequency $f_p = 12$ GHz with an RMS ac bias of $0.43 \mu\text{A}$ and $V_{\text{dc}} = hf_p/(2e)$. Cyan corresponds to bichromatic modes at frequencies f and $f_p - f$ with a width of 200 MHz. Pink corresponds to wideband photonic modes that extend from f to $f_p - f$. Experimental uncertainty (3σ) is represented as a shaded area around the average curve, '·' or '+' markers. The theory is presented using the same color with dashed lines for a dispersionless model and solid lines for a theory with a phase that increases quadratically with frequency. The black dashed horizontal line at 0dB (bottom graph) represents the vacuum level of fluctuations.

We now apply our technique to the broadband squeezed radiation generated by the tunnel junction. We show in Fig. 5 in cyan $\langle \hat{m} \rangle$ and the variance $\langle \hat{X}^2 \rangle$ of bichromatic modes centered at frequencies f and $f_p - f$ for f varying between 2.25 and 9.75 GHz. It exhibits

broadband two-mode squeezing from 4 GHz to 8 GHz. The squeezing we obtain is close to that of [5] with a much wider bandwidth, which is similar to that of the most advanced travelling wave parametric amplifiers (TWPAs)[6, 7].

The case of "white" photonic modes, which correspond to $\beta(f)$ uniform between f and $f_p - f$, is displayed in pink in Fig. 5. These modes exhibit squeezing extending from 3.5 to 8.5 GHz, starting at $\langle \hat{X}^2 \rangle \sim -1.6 \pm 0.5$ dB for a narrow band detection around 6 GHz, reaching -1.1 ± 0.3 dB for the wideband mode 5-7 GHz. $\langle \hat{X}^2 \rangle < 0$ dB is observed for modes as wide as 3.5-8.5 GHz. The squeezing obtained with the wideband mode does not go lower than that obtained with bichromatic modes, but it stays at the minimum level on a wider frequency range. This probably stems from these modes containing pairs close to 6 GHz, which are the most correlated.

Wideband modes have another remarkable property: since they involve a bandwidth much wider than the bichromatic modes, the signal to noise ratio of their measurement is much higher. For example, the bichromatic mode at 4 and 8 GHz has a bandwidth (the integrated area under $|\beta(f)|^2$) of 400 MHz while that of the wideband mode 4-8 GHz has a 10 times larger bandwidth, i.e. its measurement requires 10 times less time.

We show in Fig. 5 the theoretical expectations as dashed lines. The prediction for $\langle \hat{m} \rangle$ is remarkable, it is almost frequency independent over the whole frequency range: the junction is truly a broadband pair emitter. While theory and experiment match between 4 and 8 GHz, there is a discrepancy between both for too far apart frequencies, in particular for wideband modes. We think this is due to frequency dispersion in the detection. Phase rotation within the bandwidth of β affects the measurement. For bichromatic modes, a significant phase rotation within 200 MHz matters, but not between f and $f_p - f$. Wideband modes are more sensitive to dispersion. Adding an artificial phase rotation that grows quadratically with frequency (a linear increase corresponds to a delay, which has no influence) leads to the solid lines in Fig. 5, which fits our data for a total rotation of 5π within 1-10 GHz. Dashed and solid cyan lines are indistinguishable, in agreement with the fact that bichromatic modes very weakly sensitive to phase rotation. More experiments are needed, with a well calibrated phase response of the setup, to understand in depth the importance of dispersion in our measurement.

D. Symmetric bipartite correlations: entanglement

For applications where the key rate is important, like continuous variable quantum key distribution (CV-QKD), one might want to maximize discord [39], entanglement [24] or steering [25] (depending on the considered protocol) with a rate as large as possible. As we show below a tunnel junction is an interesting candidate for this, and our measurement method an efficient way to

measure such relevant quantities. We first compute the entanglement formation E_f and entanglement rate, in e-bits/s. For this we consider a fictitious bipartite configuration where detector A has access to frequencies below $F = 6$ GHz and detector B frequencies above F . Note that A and B could be spatially separated by the use of a diplexer, a dispersive device that does not add any noise. Bichromatic modes correspond to the usual configuration where A and B receive quasi-monochromatic signals. In contrast, for wideband modes A and B each receive broadband (up to ~ 3 GHz) signals. E_f is computed as usual from the symplectic covariance matrix between A and B , simply related to the statistics of $\langle \hat{n}_A \rangle$, $\langle \hat{n}_B \rangle$ and $\langle \hat{m} \rangle$ [24, 40, 41]. The result is presented in Fig. 6 (a) as a function of Δf . For bichromatic modes Δf is half the difference between the frequencies of A and B while for wideband modes it represents their bandwidth. We observe an entropy of formation of 0.23 at low Δf . As a comparison, a pure 2dB squeezed vacuum corresponds to $E_f = 0.3$. While E_f decreases for increasing Δf , it appears that the theoretic E_f decays much slower for wideband modes than for bichromatic ones. Note however that benefiting from the entanglement rate of bichromatic modes requires working with many detection modes, one per pair of frequencies.

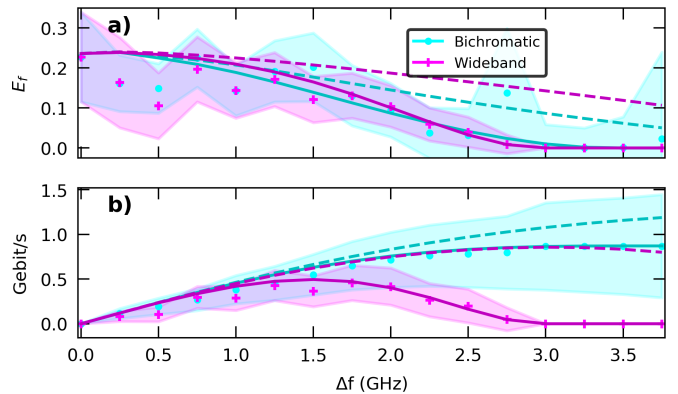


FIG. 6. The entanglement of formation E_f in bit per mode (a) and the rate of entanglement (b) in entangled bits per second as a function of difference of frequency Δf from 6 GHz. Conditions are the same as in Fig. 5. The theory is presented using the same color with dashed lines for a dispersionless model and solid lines for a theory with a phase that increases quadratically with frequency. Experimental uncertainty (3σ) is represented as a shaded area around the average curve, '.' or '+' markers.

The entanglement rate for bichromatic modes is calculated by integrating E_f over frequency [5, 7], and is shown in Fig. 6 (b). It starts by increasing linearly with the bandwidth, then saturates since increasing the bandwidth does not add entangled bits. Wideband modes are single photonic modes with a bandwidth $2\Delta f$. They carry an entanglement rate of $2E_f\Delta f$. This grows linearly with Δf and is equal to the entanglement rate of bichromatic modes at low Δf , but goes to zero at too

large Δf since E_f decays faster than $1/\Delta f$ at large bandwidth.

In Fig. 6 we report an entanglement rate of 0.87 Gbit/s (1.19 theoretical maximum) for bichromatic modes, and 0.46 Gbit/s (0.86 theoretical maximum) for wideband modes. By achieving stronger squeezing, the best reported entanglement rate in TWPAs is 2 Gbit/s [7].

While a tunnel junction provides less squeezing than the best TWPAs, it should be emphasized that its fabrication is by far less involved than that of a TWPA. Increasing the squeezing in tunnel junctions could be achieved by shaping the time-dependent excitation, with a predicted bound of -3.9 dB obtained for a periodic excitation of Dirac voltage pulses [42]. However we show in Appendix F that E_f for a two-mode vacuum squeezed state grows at best logarithmically with the squeezing intensity. Another option to increase the entanglement rate is to increase the bandwidth of the signal. The bandwidth of a tunnel junction is only limited by its RC time, here > 15 GHz. It can reach 100 GHz by working with more transparent AlO_x barrier and above 200 GHz using AlN barrier[43].

E. Asymmetric bipartite correlations: steering

In the separation of the noise generated by the junction into two detectors A and B introduced above, both detectors are not experiencing similar signals: there are more photons emitted at low frequency than at high frequency, i.e. $\langle \hat{n}_A \rangle > \langle \hat{n}_B \rangle$. This natural asymmetry exactly corresponds to the situation where quantum steering could be looked for.

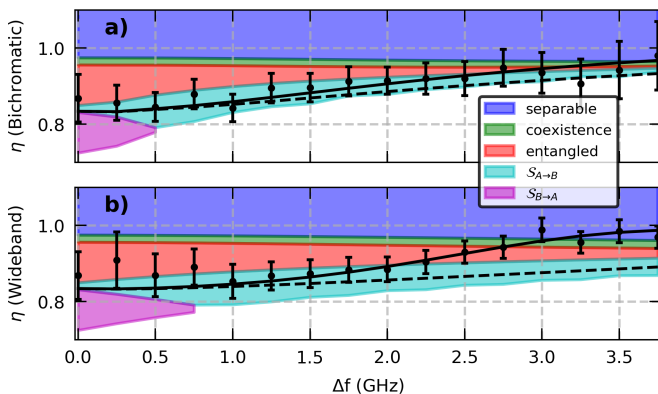


FIG. 7. Measured parameter η (black markers) as a function of the difference of frequencies Δf from 6 GHz for bichromatic states (a) and wideband states (b). Colored areas correspond to the criteria for separability and steering of bipartite Gaussian states according to [25]. The tunnel junction is excited at frequency $f_p = 12$ GHz with an RMS ac bias of $0.34 \mu\text{A}$ and $V_{dc} = hf_p/(2e)$, different from the bias that optimizes squeezing.

In [25] are given a series of criteria to know whether

a bipartite Gaussian state is separable, partially entangled or steerable, from A to B ($\mathcal{S}_{A \rightarrow B}$) or from B to A ($\mathcal{S}_{B \rightarrow A}$). These criteria require the evaluation on a single parameter $\eta = (\mu_A \mu_B)/\mu$ with μ the purity of the global state, and μ_A, μ_B those of the states detected by A and B respectively. Our detection technique allows us to calculate the purities, and so the factor η as well. We report in Fig. 7 η vs. Δf for bichromatic and wideband modes. Various colored regions correspond to the above-mentioned criteria. We clearly observe steering in the noise of the junction for bichromatic modes up to ~ 6 GHz apart and wideband modes up to 4GHz wide. In the absence of phase dispersion, steering would theoretically be possible at all Δf considered (dashed black lines in Fig. 7(b)). A previous attempt to see steering in the noise of a tunnel junction had led to a negative result [36]. Despite a similar electronic temperature, here we clearly observe steering. This is for 3 reason. First, wider modes (higher Δf) steer more easily as the theory shows. Second it seems easier to violate the steering criterion at a lower ac current than the optimal current for squeezing. In Fig. 7 the junction was ac biased by an RMS current of $0.34 \mu\text{A}$, while in Fig. 5, $I = 0.43 \mu\text{A}$. For the sake on completeness Fig. 13 in appendix G shows the measured steering in the same biasing conditions than in Fig. 5: less steering is observed in these conditions. Finally the we used the more general criterion develop in [25] valid for arbitrary bipartite Gaussian states. Steering is also observed for wideband states which will present higher key rate [25] for the same level of monomode bichromatic steering, similarly to what is observed regarding E_f and entanglement rate.

Steering (measured by a relation on purities) being a type of asymmetric quantum correlation and entanglement (measured by a going below vacuum) being symmetrical, it is natural to ask the question whether if a quantitative measure of both of them would be maximal in the same experimental conditions. This is beyond the scope of this article but should be explored in future work.

F. Asymmetric modes and criterion for inseparability

Until now we have considered bichromatic modes with equal weights on the two frequencies f_1 and f_2 . We now focus on the effect of the relative weights of two modes a_1 and a_2 by defining the combined mode:

$$\hat{d}(\lambda) = \sqrt{1-\lambda} \hat{a}_1 + \sqrt{\lambda} \hat{a}_2, \quad (15)$$

which goes from $\hat{d}(\lambda=0) = \hat{a}_1$ to $\hat{d}(\lambda=1) = \hat{a}_2$. Adding a complex phase on either of the two terms does not influence the photon statistics. As above, we consider the effect of λ on the two quantities, $\langle \hat{n} \rangle$ and $\langle \hat{X}^2 \rangle$. These considerations are reminiscent to what has been introduced by Duan et al. to construct a criterion for inseparability [44]. In this work, two EPR-like operators \hat{u} and

\hat{v} are constructed from the quadratures $\hat{x}_{1,2}$ and $\hat{p}_{1,2}$:

$$\hat{u} = |a|\hat{x}_1 + (1/a)\hat{x}_2 \quad (16)$$

$$\hat{v} = |a|\hat{p}_1 - (1/a)\hat{p}_2 \quad (17)$$

with a a real parameter. Taking $\lambda = a^4/(1 + a^4)$, the broadband quadrature \hat{X} related to \hat{d} reads $\hat{X} = (\sqrt{\lambda}/a)\hat{u}$. The definition of \hat{v} contains a minus sign while that of \hat{P} does not. For a covariance matrix that is symmetric, i.e. $\langle \hat{x}_1\hat{x}_2 \rangle = -\langle \hat{p}_1\hat{p}_2 \rangle$, one has $\langle \hat{u}^2 \rangle = \langle \hat{v}^2 \rangle$ so the criterion of Duan et al. (Eq.(3) in [44]) is simply:

$$\langle X^2 \rangle \geq \frac{1}{2}. \quad (18)$$

Thus the modes \hat{a}_1 and \hat{a}_2 being inseparable is equivalent to the combined mode \hat{d} being squeezed for certain values of λ . This result is not specific to narrow-band modes, it is valid for any two modes a_1 and a_2 . For example a_1 could cover frequencies below F and a_2 above F , as introduced for the bipartite correlations discussed above.

Below we show experimentally by varying λ that squeezing may be optimal away from $\lambda = 0.5$, i.e. for modes d with asymmetric weights. We focus on bichromatic modes with fixed frequencies $f_1 = 4.25$ GHz and $f_2 = 7.75$ GHz and show in Fig. 8a $\langle \hat{m} \rangle$ vs. λ for various ac currents in the junction. For $\lambda = 0$ and $\lambda = 1$, one has $\langle \hat{m} \rangle = 0$ since there is no pair in the detection mode. The maximum is obtained for $\lambda = 0.5$. Indeed:

$$\langle \hat{m} \rangle = 4\sqrt{\lambda(1-\lambda)}\text{Re}\langle \hat{a}_1\hat{a}_2 \rangle. \quad (19)$$

This is sound since a photon at frequency f_p gives rise to a pair of photons, one at frequency f_1 and one at frequency f_2 . The optimal detection is the one that respects this symmetry. We show in Fig.8b $\langle \hat{X}^2 \rangle$ as a function of λ

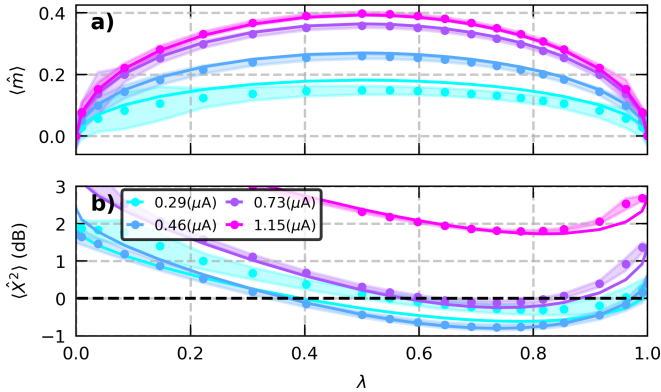


FIG. 8. $\langle \hat{m} \rangle$ in linear scale (a) and variance of the quadrature X in dB referred to vacuum (b) as a function of the parameter λ , see Eq.(15), with $f_1 = 4.25$ GHz and $f_2 = 7.75$ GHz and various ac excitations. Experimental uncertainty (1σ) is represented as a shaded area around the average curve. Markers are experimental data and solid lines theory. The black dashed horizontal line represents the vacuum level of fluctuations.

for various ac currents in the junction. For $\lambda = 0$ or

$\lambda = 1$ there is no squeezing as no photon pair is detected, thus $\langle \hat{X}^2 \rangle > 1/2$. Since $f_2 > f_1$, $\langle \hat{n}_1 \rangle > \langle \hat{n}_2 \rangle$, thus $\langle \hat{X}^2 \rangle$ is larger for $\lambda = 0$ than for $\lambda = 1$, as observed. In between there might be squeezing, as shown in Fig.5 which corresponds to $\lambda = 0.5$. This value however does not correspond to the minimum, which is clearly closer to 1 than to 0. This comes from the fact that $\langle \hat{n}_1 \rangle \neq \langle \hat{n}_2 \rangle$: the junction emits not only pairs, it also emits single photons, and more at frequency f_1 than f_2 . Thus the minimum of $\langle \hat{X}^2 \rangle$ results from a compromise between having as much pairs as possible, i.e. $\lambda = 0.5$ and having as little single photons as possible, i.e. $\lambda = 1$. More precisely:

$$\begin{aligned} \langle \hat{X}^2 \rangle &= \frac{1}{2} + (1-\lambda)\langle \hat{n}_1 \rangle + \lambda\langle \hat{n}_2 \rangle \\ &- 4\sqrt{\lambda(1-\lambda)}\text{Re}\langle \hat{a}_1\hat{a}_2 \rangle. \end{aligned} \quad (20)$$

For wideband modes, $\langle \hat{m} \rangle$ and $\langle \hat{X}^2 \rangle$ depend on the shape of the mode $\beta(f)$, both its amplitude and phase. Finding the wideband mode that optimizes $\langle \hat{m} \rangle$ or $\langle \hat{X}^2 \rangle$ is a captivating but daunting task that goes beyond the scope of this article. The same problem has been addressed with fermionic signals for which a procedure has been found [45]. Its extension to the case of a bosonic field that we are dealing with here would be of the utmost interest.

IV. CONCLUSION

We have reported an experiment able to access the photon statistics of single modes with a frequency content that may span from 1 to 10 GHz. From this we showed how to deduce squeezing spectra and how to adjust the choice of bichromatic modes for optimal detection of squeezing. Applied our technique to the broadband radiation emitted by a tunnel junction, we demonstrate squeezing over a bandwidth from 4 to 8 GHz, and show very high entanglement rate (0.87 Gbit/s measured, up to 1.19 Gbit/s achievable). We also reported the existence of quantum steering in the noise emitted by a tunnel junction. We demonstrated how the presence of squeezing in any mode is related to the presence of entanglement and how most of this entanglement can be captured by a well chosen wideband single mode.

Our technique can be applied to a large variety of wideband sources, from superconducting traveling wave parametric amplifiers (TWPAs) [5–7, 38, 46–49] to maybe the radiation generated by quantum Hall conductors [50]. Other applications are those based on a dc voltage-biased Josephson junctions, for which there is no ac excitation, so no way to measure directly the quadratures [10–14].

Our experiment opens the possibility to deal not only with pairs of frequencies but with ultra-broadband signals in general. While in the parametric downconversion process, it is quite clear that one photon at frequency f_p gives rise to a pair at frequencies symmetric around f_p , it is not clear at all that the mechanism of noise modulation

involved in electronic noise is so simple. For example, does the junction emit randomly pairs of different frequencies, or broadband pulses which contain correlation among frequencies? In the latter case there could be correlations between different pairs. Our setup is the perfect tool to answer such questions, which could provide a new viewpoint on electronic quantum transport.

ACKNOWLEDGMENTS

We are very grateful to Stéphane Virally for the many fruitful discussions, and to Gabriel Laliberté and Chris-

tian Lupien for their technical help. This work has been supported by the Canada Research Chair program, the NSERC, the Canada First Research Excellence Fund, the FRQNT, and the Canada Foundation for Innovation.

-
- [1] S. Lloyd, Enhanced Sensitivity of Photodetection via Quantum Illumination, *Science* **321**, 1463 (2008).
 - [2] S. Barzanjeh, S. Guha, C. Weedbrook, D. Vitali, J. H. Shapiro, and S. Pirandola, Microwave Quantum Illumination, *Physical Review Letters* **114**, 080503 (2015).
 - [3] The LIGO Scientific Collaboration, A gravitational wave observatory operating beyond the quantum shot-noise limit, *Nature Physics* **7**, 962 (2011).
 - [4] K. M. Backes, D. A. Palken, S. A. Kenany, B. M. Brubaker, S. B. Cahn, A. Droster, G. C. Hilton, S. Ghosh, H. Jackson, S. K. Lamoreaux, A. F. Leder, K. W. Lehnert, S. M. Lewis, M. Malnou, R. H. Maruyama, N. M. Rapidis, M. Simanovskaia, S. Singh, D. H. Speller, I. Urdinaran, L. R. Vale, E. C. van Assendelft, K. van Bibber, and H. Wang, A quantum enhanced search for dark matter axions, *Nature* **590**, 238 (2021).
 - [5] M. Esposito, A. Ranadive, L. Planat, S. Leger, D. Fraudet, V. Jouanny, O. Buisson, W. Guichard, C. Naud, J. Aumentado, F. Lecocq, and N. Roch, Observation of two-mode squeezing in a traveling wave parametric amplifier, *Phys. Rev. Lett.* **128**, 153603 (2022).
 - [6] J. Qiu, A. Grimsom, and K. P. et al., Broadband squeezed microwaves and amplification with a josephson travelling-wave parametric amplifier, *Nat. Phys.* **19**, 706–713 (2023).
 - [7] M. R. Perelshtein, K. V. Petrovnnin, V. Vesterinen, S. Hamedani Raja, I. Lilja, M. Will, A. Savin, S. Simbierowicz, R. N. Jabdaraghi, J. S. Lehtinen, L. Grönberg, J. Hassel, M. P. Prunnila, J. Govenius, G. S. Paraoanu, and P. J. Hakonen, Broadband continuous-variable entanglement generation using a kerr-free josephson metamaterial, *Phys. Rev. Appl.* **18**, 024063 (2022).
 - [8] T. Roy, S. Kundu, M. Chand, A. M. Vadiraj, A. Ranadive, N. Nehra, M. P. Patankar, J. Aumentado, A. A. Clerk, and R. Vijay, Broadband parametric amplification with impedance engineering: Beyond the gain-bandwidth product, *Applied Physics Letters* **107**, 262601 (2015).
 - [9] J. Y. Mutus, T. C. White, R. Barends, Y. Chen, Z. Chen, B. Chiaro, A. Dunsworth, E. Jeffrey, J. Kelly, A. Megrant, C. Neill, P. J. J. O’Malley, P. Roushan, D. Sank, A. Vainsencher, J. Wenner, K. M. Sundqvist, A. N. Cleland, and J. M. Martinis, Strong environmental coupling in a Josephson parametric amplifier, *Applied Physics Letters* **104**, 263513 (2014).
 - [10] S. Jebari, F. Blanchet, A. Grimm, D. Hazra, R. Albert, P. Joyez, D. Vion, D. Estève, P. F., and M. Hofheinz, Near-quantum-limited amplification from inelastic cooper-pair tunnelling, *Nat Electron* **1**, 223–227 10.1038/s41928-018-0055-7 (2018).
 - [11] C. Rolland, A. Peugeot, S. Dambach, M. Westig, B. Kubala, Y. Mukharsky, C. Altimiras, H. le Sueur, P. Joyez, D. Vion, P. Roche, D. Esteve, J. Ankerhold, and F. Portier, Antibunched photons emitted by a dc-biased josephson junction, *Phys. Rev. Lett.* **122**, 186804 (2019).
 - [12] A. Peugeot, G. Ménard, S. Dambach, M. Westig, B. Kubala, Y. Mukharsky, C. Altimiras, P. Joyez, D. Vion, P. Roche, D. Esteve, P. Milman, J. Leppäkangas, G. Johansson, M. Hofheinz, J. Ankerhold, and F. Portier, Generating two continuous entangled microwave beams using a dc-biased josephson junction, *Phys. Rev. X* **11**, 031008 (2021).
 - [13] G. C. Ménard, A. Peugeot, C. Padurariu, C. Rolland, B. Kubala, Y. Mukharsky, Z. Iftikhar, C. Altimiras, P. Roche, H. le Sueur, P. Joyez, D. Vion, D. Esteve, J. Ankerhold, and F. Portier, Emission of photon multiplets by a dc-biased superconducting circuit, *Phys. Rev. X* **12**, 021006 (2022).
 - [14] R. Albert, J. Griesmar, F. Blanchet, U. Martel, N. Bourlet, and M. Hofheinz, Microwave photon-number amplification, *Phys. Rev. X* **14**, 011011 (2024).
 - [15] J. Martin and V. Vennin, Real-space entanglement in the Cosmic Microwave Background, *Journal of Cosmology and Astroparticle Physics* **2021** (10), 036, arXiv:2106.15100 [gr-qc, physics:hep-th, physics:quant-ph].
 - [16] S. Virally and B. Reulet, Unidimensional time-domain quantum optics, *Phys. Rev. A* **100**, 023833 (2019), publisher: American Physical Society.
 - [17] G. Krauss, S. Lohss, T. Hanke, A. Sell, S. Eggert, R. Huber, and A. Leitenstorfer, Synthesis of a single cycle of light with compact erbium-doped fibre technology, *Nature Photonics* **4**, 33 (2010).
 - [18] A. Wirth, M. T. Hassan, I. Griguras, J. Gagnon, A. Moulet, T. T. Luu, S. Pabst, R. Santra, Z. A. Alahmed, A. M. Azzeer, V. S. Yakovlev, V. Pervak, F. Krausz, and E. Goulielmakis, Synthesized light transients, *Science (New York, N.Y.)* **334**, 195 (2011).

- [19] C. Riek, D. V. Seletskiy, A. S. Moskalenko, J. F. Schmidt, P. Krauspe, S. Eckart, S. Eggert, G. Burkard, and A. Leitenstorfer, Direct sampling of electric-field vacuum fluctuations, *Science* **350**, 420 (2015).
- [20] S. Onoe, S. Virally, and D. V. Seletskiy, Direct measurement of the Husimi-Q function of the electric-field in the time-domain (2023), arXiv:2307.13088 [quant-ph].
- [21] A. Bednorz, C. Bruder, B. Reulet, and W. Belzig, Non-symmetrized correlations in quantum noninvasive measurements, *Phys. Rev. Lett.* **110**, 250404 (2013).
- [22] G. Gasse, C. Lupien, and B. Reulet, Observation of squeezing in the electron quantum shot noise of a tunnel junction, *Phys. Rev. Lett.* **111**, 136601 (2013).
- [23] J.-C. Forgues, C. Lupien, and B. Reulet, Non-classical radiation emission by a coherent conductor, *Comptes Rendus Physique* **17**, 718 (2016), 1612.06337.
- [24] G. Adesso and F. Illuminati, Gaussian measures of entanglement versus negativities: The ordering of two-mode Gaussian states, *Physical Review A* **72**, 032334 (2005), arXiv:quant-ph/0506124.
- [25] I. Kogias, A. R. Lee, S. Ragy, and G. Adesso, Quantification of Gaussian Quantum Steering, *Physical Review Letters* **114**, 060403 (2015).
- [26] C. Wen, J. Wang, and J. Jing, Quantum steering for continuous variable in de Sitter space, *The European Physical Journal C* **80**, 78 (2020), arXiv:1901.04180.
- [27] S. Barnett and P. Radmore, *Methods in Theoretical Quantum Optics* (Oxford University Press, 2002).
- [28] S. Virally, J. O. Simoneau, C. Lupien, and B. Reulet, Discrete photon statistics from continuous microwave measurements, *Phys. Rev. A* **93**, 043813 (2016), 1510.03904.
- [29] J. O. Simoneau, S. Virally, C. Lupien, and B. Reulet, Photon pair shot noise in electron shot noise, *Phys. Rev. B* **95**, 060301(R) (2017).
- [30] L. Spietz, K. W. Lehnert, I. Siddiqi, and R. J. Schoelkopf, Primary Electronic Thermometry Using the Shot Noise of a Tunnel Junction, *Science* **300**, 1929 (2003).
- [31] S. T. Ruggiero, A. Williams, W. H. Rippard, A. Clark, S. W. Deiker, L. R. Vale, and J. N. Ullom, Dilute Al-Mn Alloys for Low-Temperature Device Applications, *Journal of Low Temperature Physics* **134**, 973 (2004).
- [32] J. O. Simoneau, *Mesures temporelles large bande résolues en phase du bruit de grenaille photoexcité et statistique de photons d'un amplificateur paramétrique Josephson*, Thèse, Université de Sherbrooke (2021).
- [33] J. O. Simoneau, S. Virally, C. Lupien, and B. Reulet, Photocount statistics of the josephson parametric amplifier, *Phys. Rev. Research* **4**, 013176 (2022), publisher: American Physical Society.
- [34] A. L. Grimsmo, F. Qassemi, B. Reulet, and A. Blais, Quantum optics theory of electronic noise in coherent conductors, *Phys. Rev. Lett.* **116**, 043602 (2016).
- [35] J.-C. Forgues, C. Lupien, and B. Reulet, Emission of microwave photon pairs by a tunnel junction, *Phys. Rev. Lett.* **113**, 043602 (2014).
- [36] J.-C. Forgues, C. Lupien, and B. Reulet, Experimental violation of bell-like inequalities by electronic shot noise, *Phys. Rev. Lett.* **114**, 130403 (2015).
- [37] W. Wustmann and V. Shumeiko, Parametric resonance in tunable superconducting cavities, *Phys. Rev. B* **87**, 184501 (2013).
- [38] A. L. Grimsmo and A. Blais, Squeezing and quantum state engineering with josephson travelling wave amplifiers, *npj Quantum Information* **3**, 20 (2017).
- [39] X. Su, Applying Gaussian quantum discord to quantum key distribution (2014), arXiv:1310.4253 [quant-ph].
- [40] G. Adesso, S. Ragy, and A. R. Lee, Continuous variable quantum information: Gaussian states and beyond, *Open Systems & Information Dynamics* **21**, 1440001 (2014), arXiv:1401.4679.
- [41] Q. Y. He, Q. H. Gong, and M. D. Reid, Classifying Directional Gaussian Entanglement, Einstein-Podolsky-Rosen Steering, and Discord, *Physical Review Letters* **114**, 060402 (2015).
- [42] U. C. Mendes and C. Mora, Cavity squeezing by a quantum conductor, *New Journal of Physics* **17**, 113014 (2015).
- [43] C. Lodewijk, T. Zijlstra, Shaojiang Zhu, F. Mena, A. Baryshev, and T. Klapwijk, Bandwidth Limitations of Nb/AlN/Nb SIS Mixers Around 700 GHz, *IEEE Transactions on Applied Superconductivity* **19**, 395 (2009).
- [44] L.-M. Duan, G. Giedke, J. I. Cirac, and P. Zoller, Inseparability criterion for continuous variable systems, *Phys. Rev. Lett.* **84**, 2722 (2000).
- [45] B. Roussel, C. Cabart, G. Fève, and P. Degiovanni, Processing quantum signals carried by electrical currents, *PRX Quantum* **2**, 020314 (2021).
- [46] S. Shu, N. Klimovich, B. H. Eom, A. D. Beyer, R. B. Thakur, H. G. Leduc, and P. K. Day, Nonlinearity and wide-band parametric amplification in a (nb,ti)n microstrip transmission line, *Phys. Rev. Research* **3**, 023184 (2021).
- [47] C. Macklin, K. O'Brien, D. Hover, M. E. Schwartz, V. Bolkhovskiy, X. Zhang, W. D. Oliver, and I. Siddiqi, A near-quantum-limited josephson traveling-wave parametric amplifier, *Science* **350**, 307 (2015).
- [48] L. Fasolo, A. Greco, E. Enrico, F. Illuminati, R. Lo Franco, D. Vitali, and P. Liveri, Josephson traveling wave parametric amplifiers as non-classical light source for microwave quantum illumination, *Measurement: Sensors* **18**, 100349 (2021).
- [49] M. Esposito, A. Ranadive, L. Planat, and N. Roch, Perspective on traveling wave microwave parametric amplifiers, *Measurement: Sensors* **119**, 120501 (2021).
- [50] H. Bartolomei, R. Bisognin, H. Kamata, J.-M. Berroir, E. Bocquillon, G. Ménard, B. Plaçaïs, A. Cavanna, U. Gennser, Y. Jin, P. Degiovanni, C. Mora, and G. Fève, Observation of edge magnetoplasmon squeezing in a quantum hall conductor, *Phys. Rev. Lett.* **130**, 106201 (2023).
- [51] J.-C. Forgues, F. B. Sane, S. Blanchard, L. Spietz, C. Lupien, and B. Reulet, Noise intensity-intensity correlations and the fourth cumulant of photo-assisted shot noise, *Sci Rep* **3**, 2869 (2013).

Appendix A: Numerical convolution ($\hat{v}(t) \rightarrow \hat{x}(t)$)

In order to implement the convolution (5), we need a numerical representation for the kernel $k(t)$ that properly handles the pole at $t = 0$. This is done by using the fact that the process of digitizing the signal with time step Δt implies low-pass filtering at Nyquist frequency $f_N = 1/(2\Delta t)$.

We use:

$$\begin{aligned} \frac{1}{\sqrt{|t|}} &= \int_0^{+\infty} \frac{2 \cos(2\pi f t)}{\sqrt{f}} df \\ &\approx \int_0^{f_N} \frac{2 \cos(2\pi f t)}{\sqrt{f}} df \\ &= \frac{2 \mathcal{C}(2\sqrt{f_N}|t|)}{\sqrt{|t|}}, \end{aligned}$$

where \mathcal{C} is the Fresnel cosine integral, $\mathcal{C} = \int_0^u \cos\left(\frac{\pi x^2}{2}\right) dx$. Similarly the Fresnel sine integral is $\mathcal{S} = \int_0^u \sin\left(\frac{\pi x^2}{2}\right) dx$.

Applying the same process to the case $\Theta = 0$ and $\Theta = \pi/2$ we find the discretized kernels to be:

$$\begin{aligned} k_0(n\Delta t) &\approx 2\sqrt{\frac{2f_N}{Zh}} \begin{cases} 0 & \text{if } n = 0 \\ \text{sgn}(n) \frac{\mathcal{S}(\sqrt{2|n|})}{\sqrt{|n|}} & \text{if } n \neq 0 \end{cases} \\ k_{\pi/2}(n\Delta t) &\approx 2\sqrt{\frac{2f_N}{Zh}} \begin{cases} \sqrt{2} & \text{if } n = 0 \\ \frac{\mathcal{C}(\sqrt{2|n|})}{\sqrt{|n|}} & \text{if } n \neq 0 \end{cases} \end{aligned}$$

with n integer. We chose $\Theta = 0$, i.e. we have worked with the kernel $k = k_0$.

Appendix B: Quadratures measurement

All even moments of the time dependent quadrature operator

$$\hat{x}_\Theta(t) = \frac{\hat{b}^\dagger(t)e^{i\Theta} + \hat{b}(t)e^{-i\Theta}}{\sqrt{2}} \quad (\text{B1})$$

can be split in two sums (we kept an arbitrary phase Θ for the sake of generality). The first sum contains the non-symmetric (n.s.) terms, i.e. with a different number of creation and annihilation operators in all orders; the second contains the completely symmetric (c.s.) terms, i.e. with the same number of creation and annihilation operators in all orders:

$$\begin{aligned} \hat{x}_\Theta^{2k}(t) &= \frac{1}{2^k} \sum_{l=0}^{k-1} \sum_{\text{n.s.}} \left[\hat{b}(t)^{2k-l} \hat{b}^{\dagger l}(t) e^{i\Theta(-2k+2l)} + \text{h.c.} \right] \\ &+ \frac{1}{2^k} \sum_{\text{c.s.}} \hat{b}^k(t) \hat{b}^{\dagger k}(t). \end{aligned} \quad (\text{B2})$$

The c.s. can be expressed in terms of photon number operator only [28, 29]:

$$\sum_{\text{c.s.}} = \sum_{i=0}^k \frac{(2k)!}{(i!)^2 (k-i)! 2^{k-i}} \prod_{j=0}^{i-1} (\hat{n}(t) - j).$$

Since we are only interested in $k = 1$ and 2 , we give their explicit form:

$$\begin{aligned} \hat{x}_\Theta^2(t) &= \frac{\hat{b}^2(t)e^{-i2\Theta} + \text{h.c.}}{2} + \hat{n}(t) + \frac{1}{2} \\ \hat{x}_\Theta^4(t) &= \frac{\hat{b}^4(t)e^{-i4\Theta} + \hat{b}^3(t)\hat{b}^\dagger(t)e^{-i2\Theta} + \text{h.c.}}{4} \\ &+ \frac{3}{2}\hat{n}^2(t) + \frac{3}{2}\hat{n}(t) + \frac{3}{4}. \end{aligned} \quad (\text{B3})$$

Averaging incoherently, i.e. without any synchronisation between the generation of the radiation by the ac drive in the sample and the clock of the digitization, simplifies the expressions of the c.s. and n.s. terms.

If \hat{b} describes a photon mode at frequency f , n.s. terms oscillate at frequencies $2(k-l)f$ and their time-average gives zero. This holds also for narrow-frequencies signals, so such terms were absent in [28, 29]. This is no longer true for $\hat{x}_\Theta^4(t)$ for wideband signals, as for example $\hat{b}^3(t)\hat{b}^\dagger(t)$ may contain a dc component provided the mode $\beta(f)$ is nonzero for some frequency f as well as $3f$. In the particular case of bichromatic photons at frequencies f_1 and f_2 , n.s. terms of $\hat{x}_\Theta^4(t)$ vanish upon time averaging except if $f_2 = 3f_1$. For general wideband signals, n.s. terms may contribute to the statistics of the quadratures. However for the shot noise we are considering here, n.s. terms are related to current correlators such as $\langle I(f_1)I(f_2)I(f_3)(-f_1 - f_2 - f_3) \rangle$ [34, 51] which are extremely small unless $f_1 + f_2 = f_p$ with f_p the excitation frequency. In such a case $f_1 + f_2 + f_3 > f_p$ is out of our detection bandwidth. Therefore n.s. terms never contribute here. In the absence of such terms, Θ becomes irrelevant, and we chose $\Theta = 0$.

Appendix C: Calibration

The power gain and electronic temperature T_e are continuously measured and fitted from the full spectrum of current auto-correlations, as in [32]. The slow drift in the noise temperature of the amplification chain is canceled out by interlacing experimental conditions with references ($I_{dc} = 0, I_{ac} = 0$).

The module of the gain is extracted from the shot noise of the tunnel junction (meaning the classical part of the auto-correlation, $eV \gg hf, kT$.) as is commonly done [5, 23, 30, 32]. Doing so we only recover the modulus of the gain (no phase information).

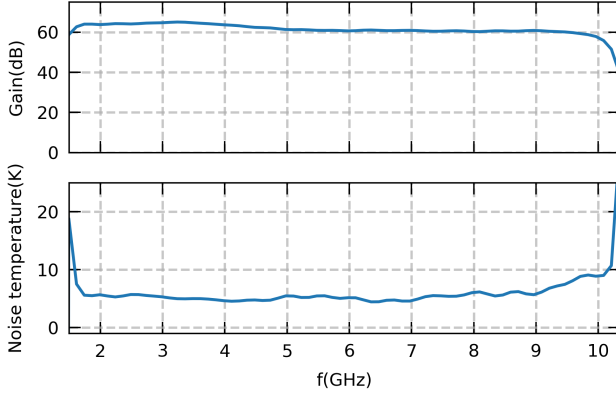


FIG. 9. Properties of the amplification chain. Top: The gain of the amplification chain (from the tunnel junction to the A/D converter.) Bottom: The noise temperature of the whole amplification chain.

Appendix D: Nonlinearities

To prevent nonlinearity in the first amplification step we ensure that the residual power from the pump is far below the 1dB compression point the LNF-LNC1-12A which is -39 dBm. About 16 dB of the pump is reflected on the sample and is attenuated by 17.5 dB by the 11 GHz low pass filter. This means that of the -78 dBm of the pump reaching the sample, only -112 dBm is reaching the first amplifier, hence no nonlinearity are expected from that amplification step. Moreover, the remaining 12 GHz is amplified by the first amplifier but falls out of the analog band of the rest of the amplification chain, so it has no influence on the measurement.

In an initial experiment we nevertheless observed nonlinearities affecting the measurement of the fourth order cumulant C_4 . In Fig. 10, we give an example of the effect of the nonlinearities on C_4 as a function of the variance C_2 , for a bichromatic 3&9 GHz mode. For vacuum fluctuations (leftmost part of the graph) and classical shot noise regime (rightmost part of the graph) C_4 should theoretically be extremely small. We see that this was not

the case.

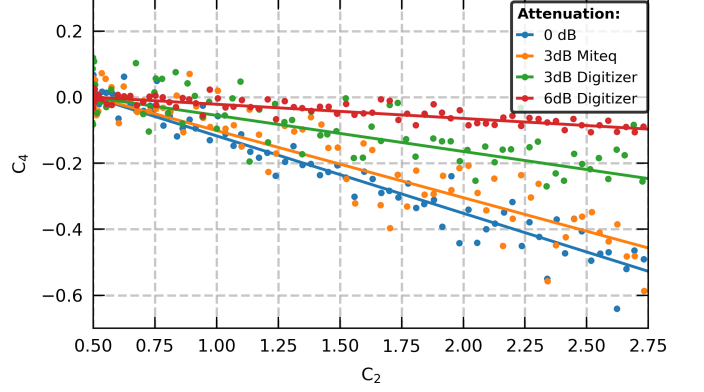


FIG. 10. Example of the effect of nonlinearities on the measurement of the 4th order cumulant as a function of the variance. The data presented is for a bichromatic 3&9 GHz mode, but is representative of the nonlinearities measured in all cases. C_2 and C_4 are cumulants of the unitless quadratures and hence are also unitless.

The setup without any additional attenuation along the amplification chain is labeled '0 dB'. If small nonlinearities are present in this regime we expect to have $C_4 \propto (C_2 + C_2^{\text{amp}})^3 \propto C_2$, as observed. C_2^{amp} is the noise of the amplifier, which is ranging from ~ 100 photons at 1GHz to ~ 10 photons at 10GHz.

Adding 3 dB of attenuation before the room temperature amplifier (1-12 GHz) and compensating with additional gain from the internal amplifier of the digitizer did not lead to any significant change in the observed nonlinearities ('3dB Miteq'). In contrast, reducing the gain of the digitizer ('3dB Digitizer', '6dB Digitizer') clearly reduces the observed nonlinearities (without impacting the noise figure of the whole amplification chain). By reducing the incident power on the A/D converter by 4 we reduce the incident voltage by 2, essentially throwing away 1 bit out of the 10 bits of the digitizer. This sacrifice in dynamic range for linearity effectively resolved all nonlinearity related issues in measurements, rendering corrections unnecessary for the presented data.

Appendix E: Electronic Temperature

We show in Fig. 11 the sample noise spectral density for several frequencies. For each frequency, by fitting the noise vs. bias we can precisely determine the electron temperature T_e . We plot in the inset of Fig. 11 the obtained T_e vs. frequency. It is almost frequency independent, and corresponds to $T_e = 17.4\text{mK}$.

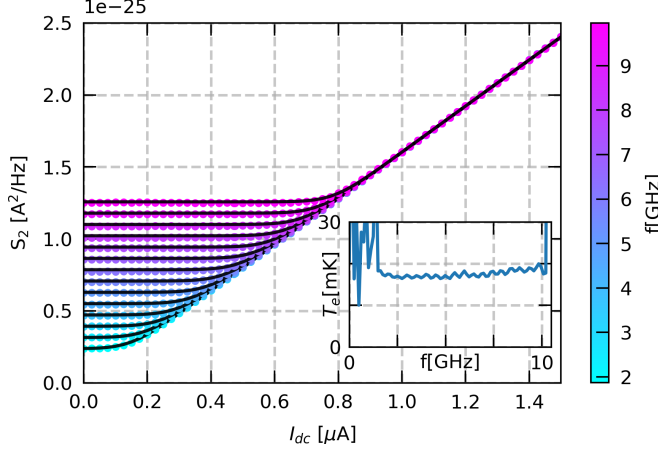


FIG. 11. Noise spectral density $S_2(f)$, of our tunnel junction as a function of the dc bias current for frequencies between 2 and 10 GHz. Dots are measurements and lines are theoretical fits. Inset : The fitted electronic temperature as a function frequency.

Appendix F: Theoretical entanglement of formation for a vacuum squeezed state.

The entanglement of formation grows at best logarithmically with the amount of squeezing for a perfect vacuum squeezed state .

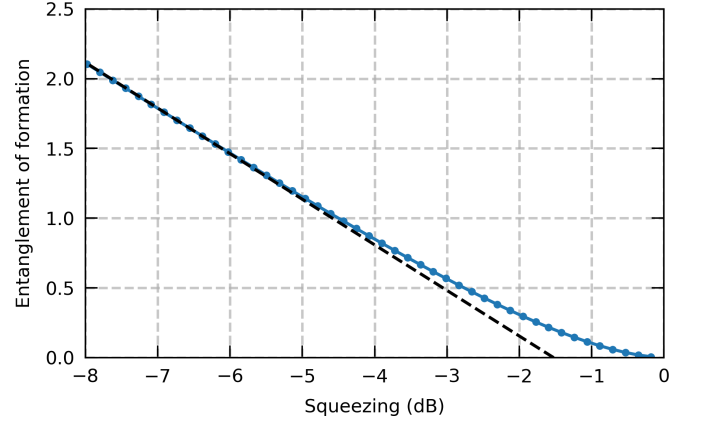


FIG. 12. Entanglement of formation for an ideal vacuum squeezed state.

Appendix G: Steering for the maximally squeezing conditions.

For completeness, here we show the results for steering at for the same conditions as in Fig. 5 which were the conditions for which the squeezing and the entanglement of formation were maximal.

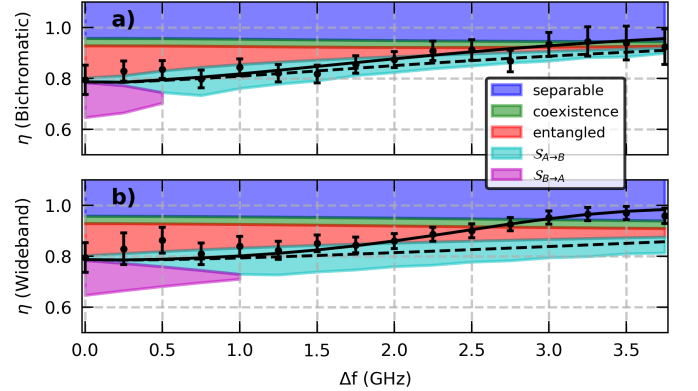


FIG. 13. Classification of separability and steering of bipartite Gaussian states using the quantification based on marginals and global purities from [25]. The measured η , '•' black markers, is presented as function of the difference of frequencies from 6 GHz for bichromatic states (a) and wideband states (b). Note that conditions where for steering are different from conditions of maximal squeezing. The tunnel junction is excited at frequency $f_p = 12$ GHz with an RMS ac bias of $0.43 \mu\text{A}$ and $V_{dc} = hf_p/(2e)$.